Journal of Colloid and Interface Science 606 (2022) 1163–1169

Contents lists available at ScienceDirect

Journal of Colloid and Interface Science

journal homepage: www.elsevier.com/locate/jcis

In situ preparation of Mn-doped perovskite nanocrystalline films and application to white light emitting devices

Xianwei Bai [a], Lingqiang Meng [a], Ni Zhou [a], Jinju Zheng [b], Xue-Feng Yu [a], Paul K. Chu [c], Jun-Jun Xiao [d], Bingsuo Zou [e,*], Jia Li [a,*]

[a] *Materials Interfaces Center, Shenzhen Institute of Advanced Technology, Chinese Academy of Sciences, Shenzhen 518055, China*
[b] *Institute of Materials, Ningbo University of Technology, Ningbo 315211, China*
[c] *Department of Physics, Department of Materials Science and Engineering, and Department of Biomedical Engineering, City University of Hong Kong, Tat Chee Avenue, Kowloon, Hong Kong, China*
[d] *College of Electronic and Information Engineering, Harbin Institute of Technology (Shenzhen), Shenzhen 518055, China*
[e] *Center on Nano-energy Research, School of Physical Science and Technology, and Guangxi Key Laboratory of Processing for Non-ferrous Metals and Featured Materials, Guangxi University, Nanning 530004, China*

GRAPHICAL ABSTRACT

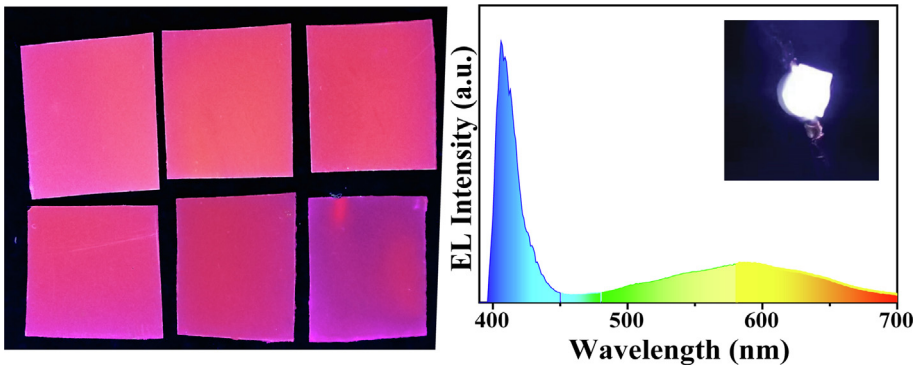

ARTICLE INFO

Article history:
Received 24 May 2021
Revised 8 August 2021
Accepted 9 August 2021
Available online 14 August 2021

Keywords:
Mn doping
Perovskite
Dual emission
Magnetic
White LED

ABSTRACT

Mn-doped perovskite nanocrystals have promised new optoelectronic applications due to their unique material properties. In the present study, Mn-doped perovskite nanocrystalline films were prepared *in situ* in a polymer matrix. The Mn-doped perovskite nanocrystals (PNCs) had good crystallinity and uniform size/spatial distributions in the polymer film. Bright dual-color emission and the long lifetime of the excited state of the dopant were observed from the host exciton and the Mn^{2+} dopant, respectively. Furthermore, magnetism was observed in the optimal Mn^{2+} concentration, implying that magnetic coupling was achieved in the Mn-doped perovskite lattice. The Mn-doped perovskite films also showed superior stability against moisture. To demonstrate the practicality of this composite film, a white light emitting device was fabricated by combining a single composite film with a blue light emitting diode; the device showed a high-quality white light emission, and the Commission Internationale De L'Eclairage (CIE) chromaticity coordinate of the white light emitting diode (WLED) (0.361, 0.326) was close to the optimal white color index. In this single-layer WLED, self-absorption among the luminous multilayers in traditional white light emitting diodes can be avoided. The study findings revealed that

* Corresponding authors.
E-mail addresses: zoubs@gxu.edu.cn (B. Zou), jia.li1@siat.ac.cn (J. Li).

https://doi.org/10.1016/j.jcis.2021.08.068

Mn-doped perovskite nanocrystalline films have many exciting properties, which bodes well for the fundamental study and design of high-performance optoelectronic devices.

1. Introduction

Perovskite semiconductors are popular in next-generation optoelectronic devices, including solar cells, [1,2,3] photodetectors, [4,5,6] lasers, [7,8,9] and light emitting diodes (LEDs). [10–14] Perovskite nanocrystals (PNCs) have high photoluminescence quantum yields (PLQYs), efficient photon absorption, and excellent optical tunability, which can be exploited by perovskite light emitting devices, such as LEDs and lasers. [15–19] To better utilize PNCs and broaden their optoelectronic applications, efforts have been made to optimize the material properties of PNCs through doping, [20,21] surface engineering, [22] and interface engineering. [23] Among these approaches, transition metal (TM) doping is an effective way to modulate the fundamental properties of PNCs. [24,25,26] Moreover, doping with Mn has attracted interest because it can endow PNCs with new optical and electronic properties as well as magnetism. [27–30] For instance, Mn-doped perovskite nanocrystals exhibit an intriguing dual-color emission from the host exciton and Mn^{2+} dopant. [31,32] Exciting optical properties and high external quantum efficiency make Mn-doped PNCs a good candidate for high-performance optoelectronic devices, including light emitting devices, photodetectors, and sensors.

Mn-doped PNCs are usually prepared by colloidal synthesis, which involves relatively complex procedures and a high processing temperature. In addition, colloidal-synthesized PNCs are prone to aggregation and precipitation in a solvent, making it difficult to produce the uniform and high-quality films required by optoelectronic applications. [33,34,35] Alternatively, *in situ* preparation of PNCs in a polymeric matrix is a good approach for forming high-quality PNC films with enhanced optoelectronic properties, especially stability. [36] However, direct *in situ* fabrication of TM-doped PNC materials in a polymeric network has not been studied in detail, even though a variety of polymer materials and un-doped PNCs have been used as building blocks to construct hybrid PNC-polymer structures.

In the present study, an *in situ* technique was designed to synthesize Mn^{2+} doped organic–inorganic hybrid perovskite nanocrystalline thin films at room temperature. Instead of casting films using pre-prepared nanocrystal suspensions, the *in situ* growth of Mn-doped PNCs was realized by incorporating the organic–inorganic hybrid perovskite precursor and the Mn^{2+} dopant in a polyvinylidene fluoride (PVDF) solution. The Mn-doped PNC films had good crystallinity and uniformity; more importantly, aggregation and precipitation were avoided. Highly stable dual-band emission was observed from the films, and the emission could have been modulated by varying the Mn^{2+} dopant concentration. The long lifetime of the excited state of Mn^{2+} was an indication of additional excellent application opportunities. Furthermore, a single Mn-doped PNC film was combined with a blue LED, creating an efficient room temperature white light emission with a CIE chromaticity coordinate of (0.361, 0.326).

2. Experimental section

2.1. Materials

Polyvinylidene fluoride (PVDF, molecular weight 10 W) was purchased from Arkema. Lead (Ⅱ) chloride ($PbCl_2$, 99%), manganese chloride ($MnCl_2$, 99%), N, *N*-dimethylformamide (DMF, greater than 99.9%) were purchased from Alfa Aesar. Hydrochloric acid (HCl, 37 wt% in water), methylamine (MA, CH_3NH_2, 33 wt% in absolute ethanol) were purchased from Aladdin. All chemicals were used as received without further purification.

2.2. Preparation of Mn-doped $MAPbCl_3$ NCs composite film and white LED

Methylammonium chloride (CH_3NH_3Cl, MACl) was synthesized by reacting methylamine with HCl. Methylamine was put in absolute ethanol, and HCl was added and stirred at 0℃ for 2 h. Afterwards, the solvent was evaporated in a rotary evaporator at a pressure of –0.1 MPa at 45℃. The precipitate was then washed three times with diethylether and vacuum-dried at 60℃ for 5 h for future use.

A composite film containing Mn-doped $MAPbCl_3$ NCs was prepared in PVDF; 0.133 mmol $MnCl_2$, 0.27 mmol MACl, 0.26 mmol $PbCl_2$, and 0.88 g of PVDF powder were introduced to 5 mL of DMF and stirred continuously at room temperature until the mixture became a clear solution. The mass fraction of the perovskite precursor was 4%-8%, [37] and the total weight of $MnCl_2$ and $PbCl_2$ remains constant at different Mn/Pb ratios. Fig. 1 shows the schematic of the preparation of the Mn-doped PNC films. The obtained solution was blade-coated onto a flat piece of glass to form a precursor solution layer with a uniform thickness, and *in situ* growth of Mn-doped PNCs in PVDF was carried out by placing the precursor solution layer in a vacuum oven at room temperature. As the DMF solvent evaporated and the precursor changed to a colorless film, the perovskite gradually crystallized, and an over-growth of nanocrystals was ruled out by gradual solidification of PVDF. Finally, the Mn-doped $MAPbCl_3$ PVDF film was peeled off from the glass plate. In the LED experiments, the Mn-doped $MAPbCl_3$/PVDF composite film was directly laid onto a blue light LED chip.

2.3. Characterization

High-resolution transmission electron microscopy (HRTEM) and transmission electron microscopy (TEM) were performed on the JEOL-JEM 2100F TEM at 200 kV, and X-ray diffraction (XRD) was conducted on the Bruker/D8 Focus X-ray diffractometer with a Cu K_α X-ray source (wavelength = 1.54 Å). The samples were scanned from 10to 60° at an increment of 5°/min. The photoluminescence (PL) spectra were measured using the F-380 fluorescence spectrometer (Tianjin Gangdong Sci. & Tech. Development Co., Ltd., China) and ultraviolet (UV)-Visible (Vis) abortion spectra of the composite films were collected on a UV-6100 UV–Vis spectrophotometer (Shanghai Mapada Instruments Co., Ltd., China). The absolute PLQY in the composite films were determined using fluorescence spectrometry with an integrated sphere (C9920-02, Hamamatsu Photonics, Japan), which was excited by an LED (F5 DIP LED, 3 V, 20 mA) at a wavelength of 365 nm for the emissive films. The time-resolved PL spectra were measured using the fluorescence lifetime measurement system (Fluromax-4P, Horiba Jobin Yvon, France) equipped with a time-correlated single-photon counting (TCSPC) spectrometer. Emission spectra of UV-pumped LEDs were measured on a spectroradiometer (PR-788, Photo Research Co. Ltd., USA).

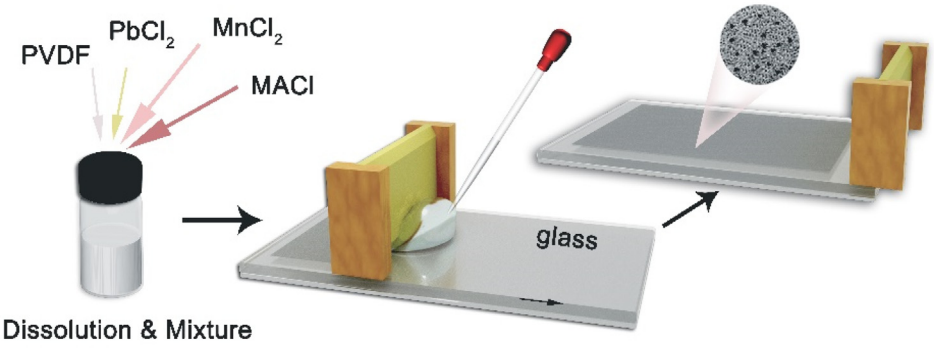

Fig. 1. Schematic illustration of the preparation procedure of Mn-doped $MAPbCl_3$ nanocrystal PVDF composite film.

3. Results and discussion

3.1. The fluorescent images of composite films

The fluorescent properties of the Mn-doped $MAPbCl_3$ PVDF film were determined, and Fig. 2a clearly shows dual-band emission due to the Mn^{2+} doping. The emission peaks at 405 nm and 590 nm stemmed from intrinsic emissions from the perovskite host and manganese ions, respectively. Fig. 2(b) shows the fluorescence images of the Mn-doped $MAPbCl_3$ composite films with different concentrations of Mn^{2+}. These samples show the obvious characteristics of manganese ions, and uniform luminescence was observed in the samples with different Mn to Pb ratios, suggesting that the Mn-doped $MAPbCl_3$ films have good quality in terms of crystallinity, dispersing properties, and uniformity.

3.2. XRD characteristics

The crystal structure of Mn-doped PNC films with different Mn to Pb ratios was characterized using XRD. As shown in Fig. 3, the XRD peaks match the typical perovskite 3D cubic structure ($Pm\bar{3}m$), [33] as shown at the bottom of Fig. 3. The broad peak at 20.7° originated from the β-phase PVDF, [36] and no additional diffraction peaks were observed, indicating the good crystallization quality. When the Mn to Pb ratios increased, the characteristic peaks at large 2θ, including (211), (022), (003), and (211), gradually disappeared; meanwhile, peaks at smaller degrees, (001), (011), and (002) decreased. These variation may be due to the change in the $MAPbX_3$ nanocrystals from an octahedral structure to an orthogonal structure, as the content of manganese increased. [33]

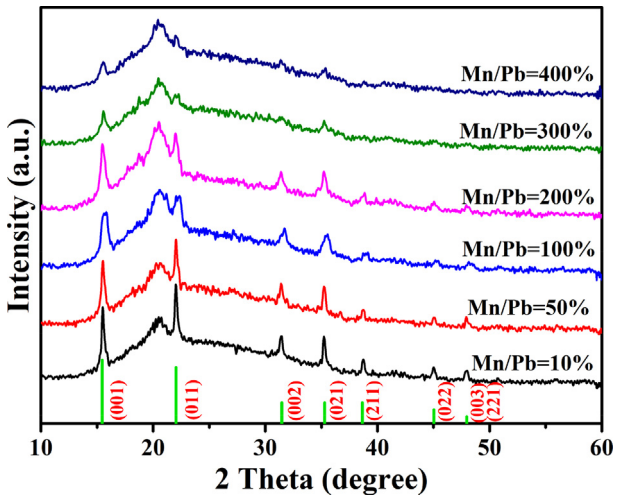

Fig. 3. XRD spectra of the Mn doped $MAPbCl_3$ composite films with different Mn to Pb ratios.

3.3. TEM characteristics

The XRD results revealed a decrease in crystallinity with more Mn^{2+} dopant, which was verified using TEM, as shown in Fig. 4. The TEM samples were prepared by spinning the diluted precursor

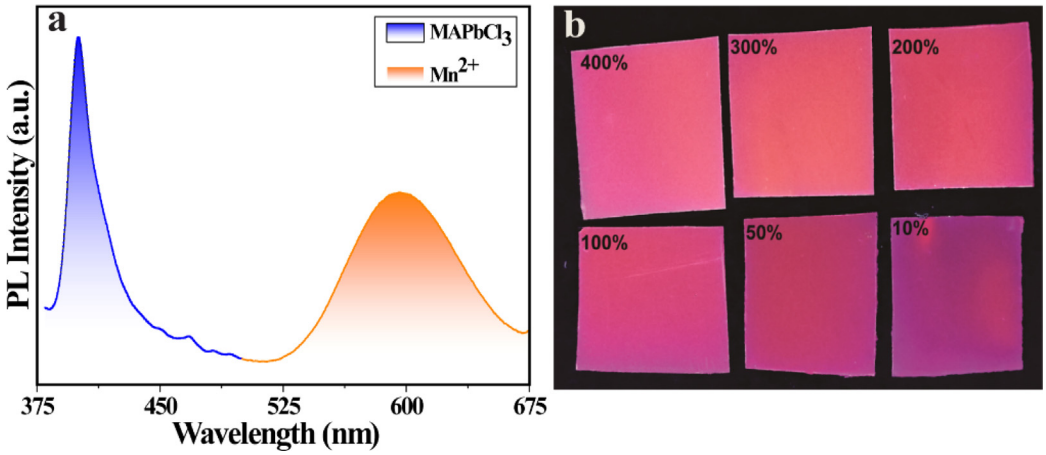

Fig. 2. (a) PL spectrum of the Mn-doped $MAPbCl_3$ composite film and (b) Fluorescent images of the composite films with the excitation wavelength of 365 nm.

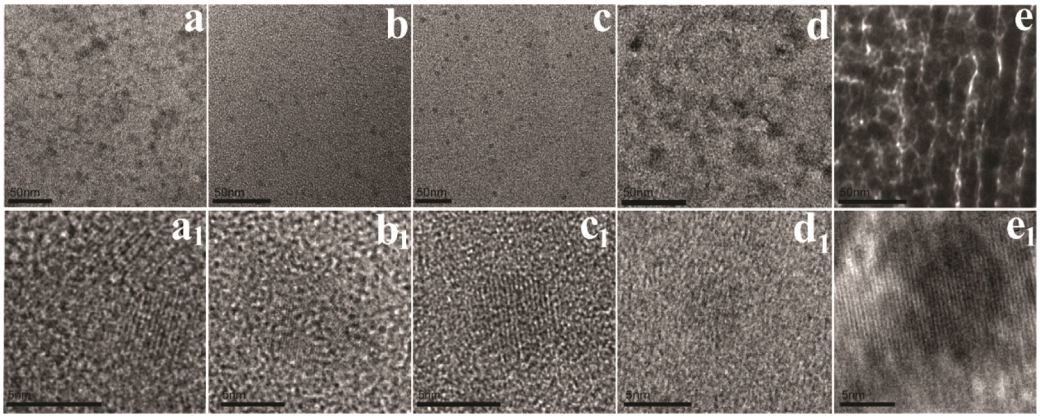

Fig. 4. (a-e) TEM images and (a1-e1) HR-TEM images of the Mn-doped $MAPbCl_3$ nanocrystals in the PVDF matrix with different Mn to Pb ratios of 0.1, 0.5, 1, 2, and 4 (Scale bar = 50 nm in the TEM images and 5 nm in the HR-TEM images).

solution on a copper net at a certain speed and drying it under a vacuum. Fig. 4a-e and 4a1-e1 display the TEM and HR-TEM images of the Mn-doped $MAPbCl_3$ nanocrystals with different Mn to Pb ratios, respectively. Obviously, the particles were smaller than 5 nm when the Mn to Pb ratio was less than 2. Fig. 4a-c and 4a1-c1 also show that the PNCs in the film had good crystallinity. In contrast, when the Mn to Pb ratio was greater than 2, the crystallinity of the PNCs decreased, as shown in Fig. 4d, e, d1, and e1. TEM confirmed that there is an optimal Mn to Pb ratio for achieving the best crystallinity, distribution, and uniform particle size.

3.4. UV–vis, PL spectra, and PLQYs characteristics

The absorbance spectra of the Mn-doped $MAPbCl_3$ films with different Pb to Mn ratios are shown in Fig. 5a. Band edge absorption of PNCs was observed in all Mn-doped $MAPbCl_3$ films. The absorption peak was at 395 nm when the molar ratio of Mn to Pb was 0.1. There was a blue shift with increasing Mn content, and the absorbance did not change significantly when the Mn to Pb ratio was greater than 0.1. The PL spectra showed clear dual-band emissions at 405 nm and 600 nm, corresponding to intrinsic emissions from the perovskite host and the manganese dopants, respectively. When the Mn to Pb ratio changed, there was no obvious shift in the excitonic emission at 405 nm; however, the PL peak from manganese blue shifted from 610 nm to 580 nm with the increasing Mn^{2+} concentration. The blue shift was caused by changes in the local crystal, such as lattice distortion, crystal symmetry, and bond length[27], which can alter the coordination of Mn^{2+}[38,39,40]. In the PNCs, manganese ions replaced lead ions in the lattice, and the crystal structure changed from the octahedral to orthogonal in the $MAPbX_3$ nanocrystals. [33] A larger Mn^{2+} concentration gave rise to a low symmetry and octahedral tilting in the $CsPbX_3$ nanocrystals, resulting in blue shifts in the manganese luminescence. [33]

In the Mn-doped perovskite system, there was an energy transfer from the perovskite host to Mn^{2+}, which was caused by the exchange coupling between the charge carriers of the perovskite host and the d electrons of Mn^{2+}. [38] Fig. 5(c) shows the PLQYs of Mn-doped PNCs for different Mn to Pb ratios. The PLQYs of the Mn-doped $MAPbCl_3$ nanocrystals increased with the manganese content when the Mn to Pb ratio was less than 2, and the PLQYs reached the maximum when the Mn to Pb ratio was 2. If the manganese content increased further, the PLQYs decreased because the crystallinity had deteriorated. Changing the MACl concentration in the composites further modified the PLQYs, as shown in Fig. 5(c). The PLQYs increased when the amount of MACl was reduced; as a result, a maximum PLQYs of 22.8% was obtained when MA:(Pb + Mn) was 0.9.

The details of PLQYs are shown in Tables S1 and S2. The maximum $PLQY_{Mn}$:$PLQY_{All}$ ratio was close to 80%, suggesting that Mn^{2+} emission dominated in the composite film. In perovskite, Mn^{2+} doping can effectively reduce a certain amount of pre-existing

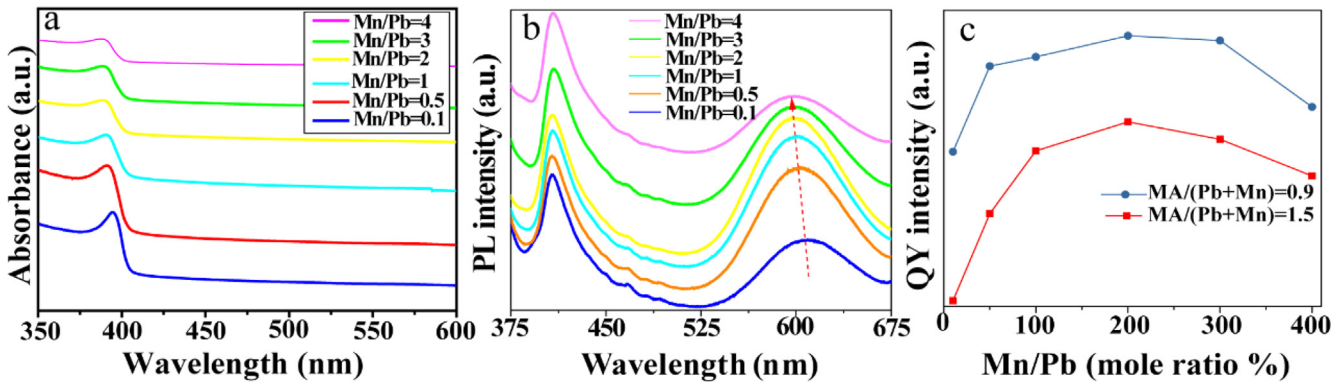

Fig. 5. (a) Absorbance spectra of the Mn-doped $MAPbCl_3$ composite films; (b) PL spectra of the composite films with various doping ratios under excitation of 365 nm; (c) Quantum yields of the Mn-doped $MAPbCl_3$ composite films with different Mn/Pb ratios and MA contents.

structural defects and serve as an efficient energy acceptor, thereby causing more efficient energy transfer from the host to Mn^{2+} and enhancing the emission properties. [41]

3.5. Time-resolved photoluminescence (TRPL)

Fig. 6 shows the TRPL curves of the $MAPbCl_3$ host emission and the Mn^{2+} emission. The host emission exhibited a double exponential decay ($y = y_0 + A_1 e^{-x1/t_1} + A_2 e^{-x2/t_2}$) behavior, leading to lifetimes of 1.23 ns (A_1 = 1.04) and 6.58 ns (A_2 = 0.03). This longer lifetime (6.58 ns) originated from carrier recombination through traps, indicating the presence of fewer defects. The smaller proportion signified that there were few traps in the Mn-doped $MAPbCl_3$ nanocrystal films, which was attributed to the passivation of surface defects by PVDF and the reduction of defects after Mn doping. [42] As shown in Fig. 6b1, the PL lifetime of the Mn ion emission displayed single exponential decay ($y = y_0 + Ae^{-x/t}$) with a lifetime of 290 ms, which was significantly enhanced in contrast to that of Mn-doped PNCs prepared in the colloidal suspension. This may be due to the less defects of nanocrystals for PVDF cladding. And the long lifetime of the dopant indicated the superior performance of Mn-doped PNCs in extracting excitonic energy for various optoelectronic applications. [43,44] The detailed PL lifetimes of the Mn ions with various Mn to Pb ratios are shown in Table S3 and Fig. S1; the maximum lifetime of the Mn ion emission was 295.05 ms for a Mn to Pb ratio of 2.

3.6. Magnetic properties

The magnetic properties of the Mn-doped $MAPbCl_3$ nanocrystals in the composite films were evaluated with the aid of a vibrating sample magnetometer (VSM) at liquid helium temperature (5 K). In the perovskite structure, manganese replaced lead at the lattice site in a strain-free crystal field; however, some Mn ions were located at the nearest neighbor Pb sites through magnetic coupling. In the case of light doping, Mn-Mn magnetic coupling was ferromagnetic; however, as the concentration of Mn ions increased, it became antiferromagnetic coupling. At a low temperature, changes in the lattice parameters resulted in partial Mn-Mn interactions inside the crystal to couple paramagnetism and ferromagnetism, as shown in Fig. 7a (Mn:Pb molar ratio of 0.1, λ_{PL} = 610-nm). In comparison, coupling between ferromagnetism and antiferromagnetism (AFM) was formed for a different Mn concentration (Mn:Pb molar ratio of more than 0.1), as shown in Fig. 7b. In the AFM case, the magnetic moments of adjacent atoms were antiparallel in the crystal lattice at low temperature, thus causing clear magnetic fluctuations in the local magnetic moments. [45,46]

3.7. Application in white LED

The practical possibility of using Mn-doped PNC films in white-light emitting devices was evaluated. Generally, a white light emitting diode (WLED) device includes blue, green, and red light emitting layers. The multiple luminous layers cause detrimental effects due to the internal self-absorption. Benefiting from the dual-band emission from the Mn-doped PNC films, the WLED can be realized by simply combining the dual-emission single film with a blue LED without using phosphors. The luminescence spectrum of the WLED device is shown in Fig. 8a, and the inset picture shows the operating WLED. The CIE chromaticity coordinate of this WLED was (0.361, 0.326), which was close to the optimal white color index, as shown in Fig. 8(b).

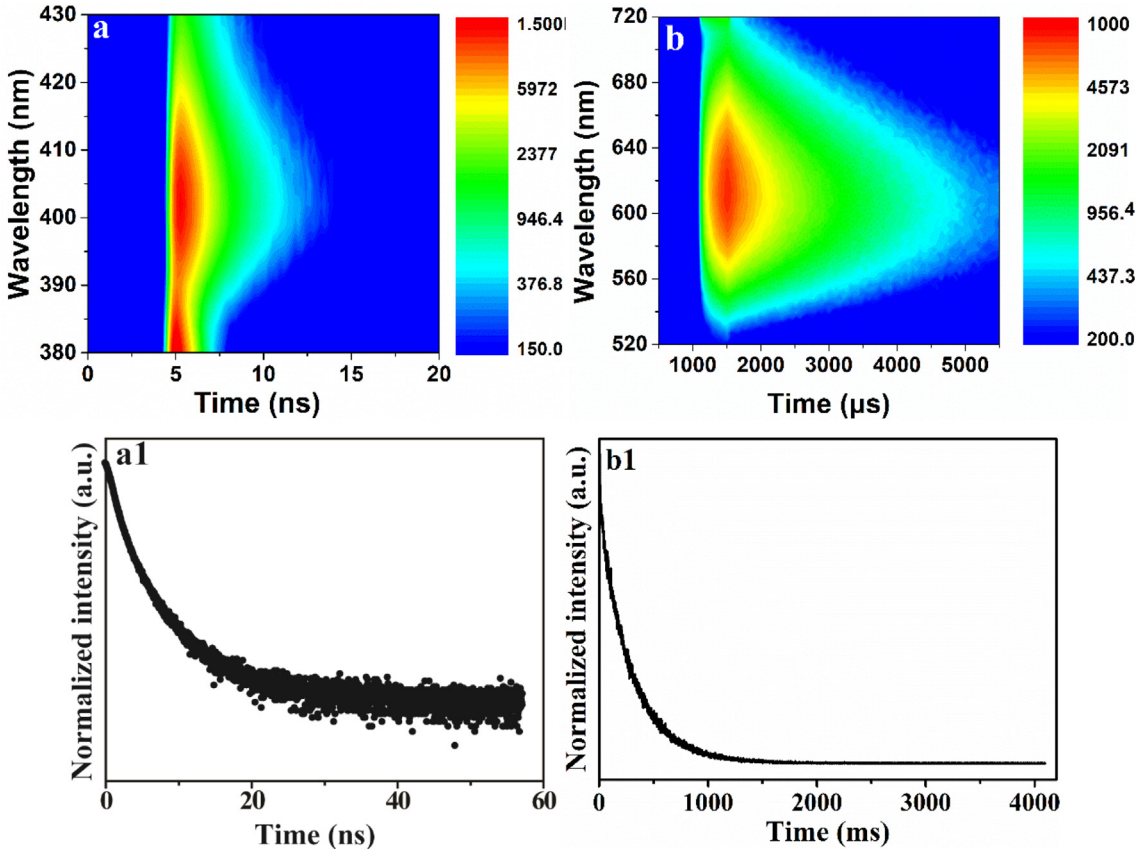

Fig. 6. Time-resolved photoluminescence spectra of Mn-doped $MAPbCl_3$ film : (a) , (a1) perovskite host emission and (b) , (b1) Mn ions emission.

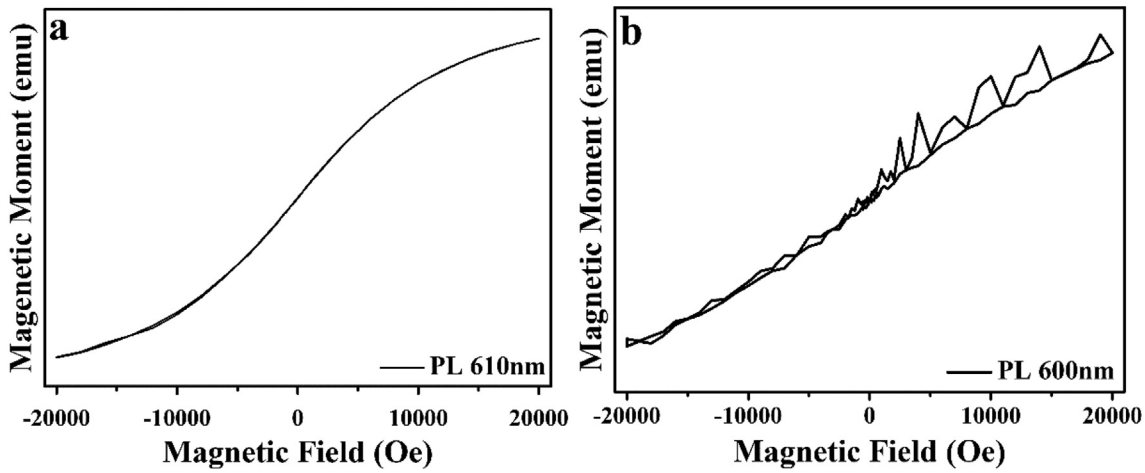

Fig. 7. Magnetic properties of the Mn-doped $MAPbCl_3$ composite films with different Mn/Pb molar ratios . (a) Mn/Pb=0.1 (PL wavelength=610 nm), (b) Mn/Pb=1 (PL wavelength=600 nm).

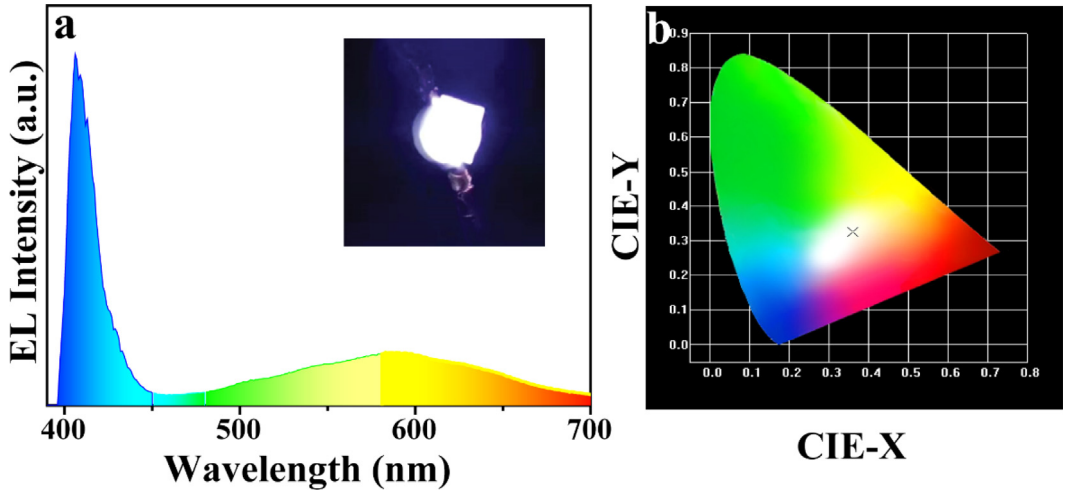

Fig. 8. (a) Emission spectrum of the white LED with the inset showing a photograph of the WLED operating at 1.6 mA; (b) CIE chromaticity coordinates of the WLED.

4. Conclusions

The present study marks the first time that a simple method was designed to realize the *in situ* preparation of Mn-doped perovskite nanocrystalline films. Due to the strong interaction between the polymer and the perovskite, the *in situ* grown Mn-doped PNCs in the hybrid films demonstrated good crystallinity and uniform distribution. Such a hybrid structure promises synergetic properties by combing the respective strengths of the perovskite host, the Mn^{2+} dopant and the polymeric framework, opening several opportunities for next-generation optoelectronic devices, as described below.

First, benefiting from the successful doping of Mn^{2+} ions in perovskite host lattices, bright dual-color emissions were observed from the host exciton and the Mn^{2+} dopant. As a result, high-quality WLED devices were realized by simply combining the hybrid film with a blue LED chip, opening up new opportunities for a high-performance liquid crystal display (LCD) backlight. Second, the PL lifetime of the Mn^{2+} dopant was significantly enhanced in contrast to that of Mn-doped PNCs prepared in the colloidal suspension, [41] implying the superior performance of Mn doped PNCs in extracting excitonic energy for various optoelectronic applications. Third, magnetism was achieved, indicating the great potential for new optoelectronic applications based on magneto-optical properties. Finally, the composite films perfectly led to the excellent stability of the hybrid materials, and the mechanic and piezoelectric properties of PVDF were well maintained, enabling the composite film to be potential multifunctional materials for flexible wearable electronics.

Declaration of Competing Interest

The authors declare that they have no known competing financial interests or personal relationships that could have appeared to influence the work reported in this paper.

Acknowledgements

This project was financially supported by the National Natural Science Foundation of China (No. 11974371) and Shenzhen Science and Technology Research Funding (Nos. JCYJ20180507182429941, JCYJ20200109115212546, and RCJC20200714114435061). The authors would like to thank Prof. Haizheng Zhong from the Beijing Institute of Technology for the valuable discussion and his help in this work.

Appendix A. Supplementary data

Supplementary data to this article can be found online at https://doi.org/10.1016/j.jcis.2021.08.068.

References

[1] Q. Jiang, Y. Zhao, X. Zhang, X. Yang, Y. Chen, Z. Chu, Q. Ye, X. Li, Z. Yin, J. You, Surface passivation of perovskite film for efficient solar cells, Nature Photon. 13 (2019) 460–466.

[2] N.J. Jeon, H. Na, E.H. Jung, T.-Y. Yang, Y.G. Lee, G. Kim, H.-W. Shin, S.I. Seok, J. Lee, J. Seo, A fluorene-terminated hole-transporting material for highly efficient and stable perovskite solar cells, Nat. Energy. 3 (2018) 682–689.

[3] Q.-D. Yang, J. Li, Y. Cheng, H.-W. Li, Z. Guan, B. Yu, S.-W. Tsang, Graphene oxide as an efficient hole-transporting material for high-performance perovskite solar cells with enhanced stability, J. Mater. Chem. A. 5 (2017) 9852–9858.

[4] M.I. Saidaminov, V. Adinolfi, R. Comin, A.L. Abdelhady, W. Peng, I. Dursun, M. Yuan, S. Hoogland, E.H. Sargent, O.M. Bakr, Planar-integrated single-crystalline perovskite photodetectors. Nat. commun. 6 (2015) 1–7.

[5] H. Wang, D.H. Kim, Perovskite-based photodetectors: materials and devices, Chem. Soc. Rev. 46 (2017) 5204–5236.

[6] Y. Gao, Y. Ge, X. Wang, J. Liu, W. Liu, Y. Cao, K. Gu, Z. Guo, Y.M. Wei, N. Zhou, Ultrathin and Ultrasensitive Direct X-ray Detector Based on Heterojunction Phototransistors, Adv. Mater. 33 (2021) 2101717.

[7] S.A. Veldhuis, P.P. Boix, N. Yantara, M. Li, T.C. Sum, N. Mathews, S.G. Mhaisalkar, Perovskite materials for light-emitting diodes and lasers, Adv. Mater. 28 (2016) 6804–6834.

[8] Y. Wang, X. Li, V. Nalla, H. Zeng, H. Sun, Solution-processed low threshold vertical cavity surface emitting lasers from all-inorganic perovskite nanocrystals, Adv. Funct. Mater. 27 (2017) 1605088.

[9] L. Jiang, R. Liu, R. Su, Y. Yu, H. Xu, Y. Wei, Z.-K. Zhou, X. Wang, Continuous wave pumped single-mode nanolasers in inorganic perovskites with robust stability and high quantum yield, Nanoscale. 10 (2018) 13565–13571.

[10] Y. Ling, Y. Tian, X. Wang, J.C. Wang, J.M. Knox, F. Perez-Orive, Y. Du, L. Tan, K. Hanson, B. Ma, Enhanced optical and electrical properties of polymer-assisted all-inorganic perovskites for light-emitting diodes, Adv. Mater. 28 (2016) 8983–8989.

[11] J. Xing, Y. Zhao, M. Askerka, L.N. Quan, X. Gong, W. Zhao, J. Zhao, H. Tan, G. Long, L. Gao, Color-stable highly luminescent sky-blue perovskite light-emitting diodes, Nat. commun. 9 (2018) 1–8.

[12] M. Bidikoudi, E. Fresta, R. Costa, White perovskite based lighting devices, Chem. Comm. 54 (2018) 8150–8169.

[13] F. Zhang, H. Zhong, C. Chen, X.-G. Wu, X. Hu, H. Huang, J. Han, B. Zou, Y. Dong, Brightly luminescent and color-tunable colloidal $CH_3NH_3PbX_3$ (X= Br, I, Cl) quantum dots: potential alternatives for display technology, Acs Nano. 9 (2015) 4533–4542.

[14] G. Zhou, X. Jiang, M. Molokeev, Z. Lin, J. Zhao, J. Wang, Z. Xia, Optically modulated ultra-broad-band warm white emission in Mn^{2+}-doped ($C_6H_{18}N_2O_2$) PbBr 4 hybrid metal halide phosphor, Chem. Mater. 31 (2019) 5788–5795.

[15] S. Chang, Z. Bai, H. Zhong, In situ fabricated perovskite nanocrystals: a revolution in optical materials, Adv. Opt. Mater. 6 (2018) 1800380.

[16] Z. Yuan, Y. Miao, Z. Hu, W. Xu, C. Kuang, K. Pan, P. Liu, J. Lai, B. Sun, J. Wang, Unveiling the synergistic effect of precursor stoichiometry and interfacial reactions for perovskite light-emitting diodes, Nat. commun. 10 (2019) 1–9.

[17] Y. Miao, Y. Ke, N. Wang, W. Zou, M. Xu, Y. Cao, Y. Sun, R. Yang, Y. Wang, Y. Tong, Stable and bright formamidinium-based perovskite light-emitting diodes with high energy conversion efficiency, Nat. commun. 10 (2019) 1–7.

[18] Q. Shang, M. Li, L. Zhao, D. Chen, S. Zhang, S. Chen, P. Gao, C. Shen, J. Xing, G. Xing, Role of the exciton–polariton in a continuous-wave optically pumped $CsPbBr_3$ perovskite laser, Nano Lett. 20 (2020) 6636–6643.

[19] H. Huang, J. Li, Y. Yi, J. Wang, Y. Kang, P.K. Chu, H. Ong, X.-F. Yu, In situ growth of all-inorganic perovskite nanocrystals on black phosphorus nanosheets, Chem. Commun. 54 (2018) 2365–2368.

[20] R. Begum, M.R. Parida, A.L. Abdelhady, B. Murali, N.M. Alyami, G.H. Ahmed, M. N. Hedhili, O.M. Bakr, O.F. Mohammed, Engineering interfacial charge transfer in $CsPbBr_3$ perovskite nanocrystals by heterovalent doping, J. Am. Chem. Soc. 139 (2017) 731–737.

[21] T. Qiao, D. Parobek, Y. Dong, E. Ha, D.H. Son, Photoinduced Mn doping in cesium lead halide perovskite nanocrystals, Nanoscale. 11 (2019) 5247–5253.

[22] J. Pan, L.N. Quan, Y. Zhao, W. Peng, B. Murali, S.P. Sarmah, M. Yuan, L. Sinatra, N. M. Alyami, J. Liu, Highly efficient perovskite-quantum-dot light-emitting diodes by surface engineering, Adv. Mater. 28 (2016) 8718–8725.

[23] M.M. Tavakoli, M. Saliba, P. Yadav, P. Holzhey, A. Hagfeldt, S.M. Zakeeruddin, M. Grätzel, Synergistic crystal and interface engineering for efficient and stable perovskite photovoltaics, Adv. Ener. Mater. 9 (2019) 1802646.

[24] G. Pan, X. Bai, D. Yang, X. Chen, P. Jing, S. Qu, L. Zhang, D. Zhou, J. Zhu, W. Xu, Doping lanthanide into perovskite nanocrystals: highly improved and expanded optical properties, Nano Lett. 17 (2017) 8005–8011.

[25] Z.-J. Yong, S.-Q. Guo, J.-P. Ma, J.-Y. Zhang, Z.-Y. Li, Y.-M. Chen, B.-B. Zhang, Y. Zhou, J. Shu, J.-L. Gu, Doping-enhanced short-range order of perovskite nanocrystals for near-unity violet luminescence quantum yield, J. Am. Chem. Soc. 140 (2018) 9942–9951.

[26] K. Xing, X. Yuan, Y. Wang, J. Li, Y. Wang, Y. Fan, L. Yuan, K. Li, Z. Wu, H. Li, Improved doping and emission efficiencies of Mn-doped $CsPbCl_3$ perovskite nanocrystals via nickel chloride, J. Phy. Chem. lett. 10 (2019) 4177–4184.

[27] W. Liu, Q. Lin, H. Li, K. Wu, I. Robel, J.M. Pietryga, V.I. Klimov, Mn^{2+}-doped lead halide perovskite nanocrystals with dual-color emission controlled by halide content, J. Am. Chem. Soc. 138 (2016) 14954–14961.

[28] W.J. Mir, A. Swarnkar, A. Nag, Postsynthesis Mn-doping in $CsPbI_3$ nanocrystals to stabilize the black perovskite phase, Nanoscale. 11 (2019) 4278–4286.

[29] W.J. Mir, M. Jagadeeswararao, S. Das, A. Nag, Colloidal Mn-doped cesium lead halide perovskite nanoplatelets, ACS Ener. Lett. 2 (2017) 537–543.

[30] B. Su, G. Zhou, J. Huang, E. Song, A. Nag, Z. Xia, Mn^{2+}-Doped Metal Halide Perovskites: Structure, Photoluminescence, and Application, Laser & Photonics Rev. 15 (2021) 2000334.

[31] D. Parobek, B.J. Roman, Y. Dong, H. Jin, E. Lee, M. Sheldon, D.H. Son, Exciton-to-dopant energy transfer in Mn-doped cesium lead halide perovskite nanocrystals, Nano Lett. 16 (2016) 7376–7380.

[32] Q. Sun, S. Wang, C. Zhao, J. Leng, W. Tian, S. Jin, Excitation-dependent emission color tuning from an individual Mn-doped perovskite microcrystal, J. Am. Chem. Soc. 141 (2019) 20089–20096.

[33] P. Arunkumar, K.H. Gil, S. Won, S. Unithrattil, Y.H. Kim, H.J. Kim, W.B. Im, Colloidal organolead halide perovskite with a high Mn solubility limit: a step toward Pb-free luminescent quantum dots, J. Phys. Chem. lett. 8 (2017) 4161–4166.

[34] S. Zou, Y. Liu, J. Li, C. Liu, R. Feng, F. Jiang, Y. Li, J. Song, H. Zeng, M. Hong, Stabilizing cesium lead halide perovskite lattice through Mn (II) substitution for air-stable light-emitting diodes, J. Am. Chem. Soc. 139 (2017) 11443–11450.

[35] C. Bi, S. Wang, Q. Li, S.V. Kershaw, J. Tian, A.L. Rogach, Thermally stable copper (II)-doped cesium lead halide perovskite quantum dots with strong blue emission, J. Phys. chem. lett. 10 (2019) 943–952.

[36] Q. Zhou, Z. Bai, W.g. Lu, Y. Wang, B. Zou, H. Zhong, In situ fabrication of halide perovskite nanocrystal-embedded polymer composite films with enhanced photoluminescence for display backlights. Adv. Mater. 28 (2016) 9163-9168.

[37] W.G. Lu, X.G. Wu, S. Huang, L. Wang, Q. Zhou, B. Zou, H. Zhong, Y. Wang, Strong Polarized Photoluminescence from Stretched Perovskite-Nanocrystal-Embedded Polymer Composite Films, Adv. Opt. Mater. 5 (2017) 1700594.

[38] T. Zuo, Z. Sun, Y. Zhao, X. Jiang, X. Gao, The big red shift of photoluminescence of Mn dopants in strained CdS: A case study of Mn-doped MnS– CdS heteronanostructures, J. Am. Chem. Soc. 132 (2010) 6618–6619.

[39] A. Hazarika, A. Layek, S. De, A. Nag, S. Debnath, P. Mahadevan, A. Chowdhury, D.D. Sarma, Ultranarrow and widely tunable Mn^{2+}-induced photoluminescence from single Mn-doped nanocrystals of ZnS-CdS alloys, Phys. Rev. Lett. 110 (2013) 267401.

[40] X. Bai, H. Zhong, B. Chen, C. Chen, J. Han, R. Zeng, B. Zou, Pyridine-modulated Mn ion emission properties of $C_{10}H_{12}N_2MnBr_4$ and $C_5H_6NMnBr_3$ single crystals, J. Phys. Chem. C. 122 (2018) 3130–3137.

[41] L. Fei, X. Yuan, J. Hua, M. Ikezawa, R. Zeng, H. Li, Y. Masumoto, J. Zhao, Enhanced luminescence and energy transfer in Mn^{2+} doped $CsPbCl_{3-x}$ Br x perovskite nanocrystals, Nanoscale. 10 (2018) 19435–19442.

[42] D. Rossi, D. Parobek, Y. Dong, D.H. Son, Dynamics of exciton–Mn energy transfer in Mn-doped $CsPbCl_3$ perovskite nanocrystals, J. Phys. Chem. C. 121 (2017) 17143–17149.

[43] P. Kr, R. Viswanatha, Mechanism of Mn emission: Energy transfer vs charge transfer dynamics in Mn-doped quantum dots, APL Mater. 8 (2020) 020901.

[44] M. He, Y. Cheng, L. Shen, C. Shen, H. Zhang, W. Xiang, X. Liang, Mn-doped $CsPbCl_3$ perovskite quantum dots (PQDs) incorporated into silica/alumina particles used for WLEDs, Appl. Surf. Sci. 448 (2018) 400–406.

[45] Z. Yin, S. Lebegue, M.-J. Han, B. Neal, S. Savrasov, W. Pickett, Electron-hole symmetry and magnetic coupling in antiferromagnetic LaFeAsO, Phys. Rev. Lett. 101 (2008) 047001.

[46] O. Shpyrko, E. Isaacs, J. Logan, Y. Feng, G. Aeppli, R. Jaramillo, H. Kim, T. Rosenbaum, P. Zschack, M. Sprung, Direct measurement of antiferromagnetic domain fluctuations, Nature. 447 (2007) 68–71.